Enhanced Photocatalytic Activity of Ce^{3+}-TiO_2 for 2-Mercaptobenzothiazole Degradation in Aqueous Suspension for Odour Control

F. B. Li[1, 2], X. Z. Li[1*], M. F. Hou[2], K. W. Cheah[3] and W. C. H. Choy[3]

[1]Department of Civil and Structural Engineering, The Hong Kong Polytechnic University, Hong Kong, China

[2]Guangdong Key Laboratory of Agricultural Environment Pollution Integrated Control, Guangdong Institute of Eco-Environment and Soil Science, Guangzhou, 510650, China

[3]Department of Physics, Hong Kong Baptist University, Hong Kong, China

Abstract: A series of cerium ion-doped titanium dioxide (Ce^{3+}-TiO_2) catalysts with special 4*f* electron configuration was prepared by a sol-gel process and characterized by Brunauer-Emmett-Teller method, X-ray diffraction, X-ray photoelectron spectroscopy (XPS), UV-visible diffuse reflectance spectroscopy (DRS), and also photoluminescence (PL) emission spectroscopy. The photocatalytic activity of Ce^{3+}-TiO_2 catalysts was evaluated in the 2-mercaptobenzothiazole (MBT) degradation in aqueous suspension under UV or visible light illumination. The experimental results demonstrated that the overall photocatalytic activity of Ce^{3+}-TiO_2 catalysts in MBT degradation was signigicantly enhanced due to higher adsorption capacity and better separation of electron-hole pairs. The experimental results verified that both the adsorption equilibrium constant (K_a) and the saturated adsorption amount (Γ_{max}) increased with the increase of cerium ion content. The results of XPS analysis showed that the Ti^{3+}, Ce^{3+}, and Ce^{4+} ions reside in the Ce^{3+}-TiO_2 catalysts. The results of DRS analysis indicated that the Ce^{3+}-TiO_2 catalysts had significant optical absorption in the visible region between 400-500 nm because electrons could be excited from the valence band of TiO_2 or ground state of cerium oxides to Ce 4*f* level. In the meantime, the dependence of the electron-hole pair separation on cerium ion content was investigated by the PL analysis. It was found that the separation efficiency of electron-hole pairs increased with the increase of cerium ion content at first and then decreased when the cerium ion content exceeded its optimal value. It is proposed that the formation of two sub-energy levels (defect level and Ce 4*f* level) in Ce^{3+}-TiO_2 might be a critical reason to eliminate the recombination of electron-hole pairs and to enhance the photocatalytic activity.

Keywords: Adsorption; Cerium ion; Titanium dioxide; 2-mercaptobenzothiazole; Visible light

[*] *To whom correspondence should be addressed. Fax: (852) 2334 6389; Email: cexzli@polyu.edu.hk*

1. Introduction

TiO_2-based photocatalytic oxidation techniques have received much attention thanks to their application potential for complete mineralization of many toxic and non-biodegradable organics [1-3]. Some studies indicated that the photocatalytic activity of TiO_2 catalysts depends strongly on two factors: adsorption behavior and the separation efficiency of electron-hole pairs [1-3]. The adsorption capacity can be generally improved by adjusting the surface-zero-charge point or by increasing the specific surface area and pore volume of catalysts [4-6]. On the other hand, it has been reported that doping with a group of transitional metal ions [5-11] or depositing some noble metals such as Au [4, 12-14] and Pt [15], or coupling metallic oxides [16-19] with *d* electronic configuration into TiO_2 lattice could eliminate the recombination of electron-hole pairs significantly and also result in the extension of their wavelength response toward the visible region [20].

Alternatively, the photocatalytic activity of TiO_2 could be significantly enhanced by doping with lanthanide ions/oxides with 4*f* electron configurations because lanthanide ions could form complexes with various Lewis bases including organic acids, amines, aldehydes, alcohols, and thiols in the interaction of the functional groups with their *f*-orbital [21-22]. Ranjit et al. [21-22] reported the increase of saturated adsorption capacity and the adsorption equilibrium constant simultaneously for salicylic acid, *t*-cinnamic acid, and *p*-chlorophenoxy-acetic acid owing to the Eu^{3+}, Pr^{3+}, or Yb^{3+} doping. Xie et al. [23] reported Nd^{3+}-TiO_2 sol catalysts had photocatalytic activity for phenol degradation under visible light irradiation. However, the effect of lanthanide oxides on the separation of electron-hole pairs under visible light irradiation and the photoresponse had seldom been investigated in these publications. Among the lanthanide oxides, the catalytic properties of ceria have received much attention due to two features of (1) the redox couple Ce^{3+}/Ce^{4+} with the ability of ceria to shift between CeO_2 and Ce_2O_3 under oxidizing and reducing conditions; and (2) the easy formation of labile oxygen vacancies (OV) with the relatively high mobility of bulk oxygen species [18]. Furthermore, the different electronic structures of the Ce^{3+} with $4f^1 5d^0$ and the Ce^{4+} with $4f^0 5d^0$

would lead to different optical properties [24-25] and dissimilar catalytic properties for CeO_2 and CeO_x-TiO_2 and also Ce^{3+}-TiO_2 [26-27].

In this study, Ce^{3+}-TiO_2 catalysts were prepared by a sol-gel method and 2-mercaptobenzothiazole (MBT) was used as a model chemical to carry out the photocatalytic activity tests under UV or visible light irradiation. MBT is an odorous chemical with a –SH group and isolated electron pairs, which has no optical absorption band in the visible region. The aim of this study was at investigating the effects of cerium ion doping on (1) investigating the contribution of adsorption ability and the separation of electron-hole pairs to the enhancement of apparent photocatalytic activity under either UV or visible light irradiation; (2) eventually disclosing the mechanisms of photocatalytic activity enhancement due to cerium ion doping.

2. Experimental Section

2.1 Preparation of Ce^{3+}-TiO_2 Catalysts

The cerium ion-doped titanium dioxide (Ce^{3+}-TiO_2) catalysts were prepared by a sol-gel process with the following procedure: 17 mL of tetra-n-butyl titanium ($Ti(O\text{-}Bu)_4$) was dissolved into 80 mL of absolute ethanol; then the $Ti(O\text{-}Bu)_4$ solution was added drop-wise under vigorous stirring into 100 mL of a mixture solution containing 84 mL of ethanol (95%), 1 mL of 0.1 M $Ce(NO_3)_3$, and 15 mL of acetic acid (>99.8%); the resulting transparent colloidal suspension was stirred for 2 h and aged for 2 d untill the formation of gel; the gel was dried at 253 K under vacuum and then ground to form semisolid powder; the powder was calcined at 773 K for 2 h to form the Ce^{3+}-TiO_2 powder eventually. This Ce^{3+}-TiO_2 catalyst had a nominal atomic ratio (Ce/Ti) of 0.2%, so it is named 0.2% Ce^{3+}-TiO_2 in this study. Accordingly, other $Ce^{3+}TiO_2$ samples containing different cerium ion contents were named 0.7% Ce^{3+}-TiO_2, 1.2% Ce^{3+}-TiO_2, and 2.0% Ce^{3+}-TiO_2, respectively.

2.2 Characterization of Ce^{3+}-TiO_2 Catalysts

To determine the crystal phase composition of the prepared Ce^{3+}-TiO_2 samples, we carried out X-ray diffraction (XRD) measurements at room temperature using a Rigaku D/MAX-IIIA diffractometer with CuK_α radiation (λ = 0.15418 nm). The accelerating voltage of 30 kV and emission current of 30 mA were used. The specific surface area of the catalysts was measured by the dynamic Brunauer-Emmett-Teller (BET) method, in which a N_2 gas was adsorbed at 77 K using a Carlo Erba Sorptometer. To study the light absorption of the catalysts, the diffuse reflectance spectra (DRS) of the catalyst samples in the wavelength range of 200-800 nm were obtained using a UV-visible scanning spectrophotometer (Shimadzu UV-2101 PC), while $BaSO_4$ was used as a reference. To study the recombination of electrons/holes, the photoluminescence (PL) emission spectra of the catalyst samples were measured with the following procedure: at either room temperature or 77 K, a 325 nm He-Cd laser was used as an excitation light source; the light from the sample was focused into a spectrometer (Spex500) and detected by a photo-multiplier tube (PMT); the signal from the PMT was inputted to a photon counter (SR400) before recorded by a computer. To study the valance band state and chemical state of the photocatalysts, we received the X-ray photoelectron spectroscopy (XPS) results of the catalyst samples with the PHI Quantum ESCA microprobe system, using the MgK_α line of a 250-W Mg X-ray tube as a radiation source with the energy of 1253.6 eV, 16 mA × 12.5 kV and the working pressure of lower than 1×10^{-8} N m^{-2}. As an internal reference for the absolute binding energy, the C 1s peak at 284.80 eV of hydrocarbon contaminantion was used. The fitting of XPS curves was analyzed with a software package (Multipak 6.0A).

2.3 MBT Adsorption Experiment

MBT chemical was provided by BDH and was used as a model odorous substrate in this study without further purification. To determine the adsorption behavior of Ce^{3+}-TiO_2 catalysts, we performed a set of adsorption isotherm tests in the dark. In each test, to 10 mL of MBT suspension was added 0.1 g of Ce^{3+}-TiO_2 powder and the mixture was then put into a shaker operating at 130

revolutions min^{-1} for 24 h at 298 ± 1 K. The MBT concentration in the suspension before and after the adsorption tests was analyzed and the adsorbed amount of MBT on the catalysts was calculated based on a mass balance.

2.4 MBT Photocatalytic Degradation Experiment

A Pyrex cylindrical photoreactor was used to conduct photocatalytic oxidation experiments, in which an 8-W UVA lamp (Luzchem Research, Inc.) with a special emission peak at 365 nm was positioned at the centre of the cylindrical vessel and was used for photoreaction under UV irradiation, while a 110-W high-pressure sodium lamp with main emission in the range of 400-800 nm was used for photoreaction under visible light irradiation. The UV light portion of sodium lamp was filtered by 0.5 M $NaNO_2$ solution. This cylindrical photoreactor was surrounded by a Pyrex circulating water jacket to control the temperature during the reaction. The reaction suspension was prepared by adding 0.25 g of Ce^{3+}-TiO_2 powder into 250 mL of aqueous MBT solution. Prior to photoreaction, the suspension was magnetically stirred in the dark for 30 min to approach adsorption/desorption equilibrium. The aqueous suspension containing MBT and Ce^{3+}-TiO_2 was aerated with a constant air flow. At the given time intervals, the analytical samples were taken from the suspension and immediately centrifuged for 20 min, and then filtered through a 0.45-μm Millipore filter to remove particles.

2.5 Analytical Method

The MBT concentration in aqueous solution was determined by LC, which consists of a gradient pump (Spectra System P4000), an autosampler (Spectra System Tem AS3000) with a 20 μl injection loop, a Thermo Ques Hypersil ODS column (C18, 5 μm, 250 × 4.6 mm ID) and a photodiode array UV detector (Spectra System UV6000LP). While a mobile phase (70% methanol and 30% water with 1% acetic acid) was operated at a flow rate of 0.5 ml min^{-1}, a maximum absorption wavelength of 323 nm was selected to detect MBT.

3. Results and Discussion

3.1 Adsorption Behavior

To study the adsorption ability of TiO_2 catalysts affected by cerium ion doping, we carried out a set of MBT adsorption tests in the dark. The experimental data obtained in the adsorption tests were well fitted by the Langmuir equation [28]. The MBT adsorption isotherms are shown in Fig. 1. In the meantime, the saturated adsorption amount (Γ_{max}) and the adsorption equilibrium constant (K_a) of MBT onto the different catalysts were calculated and are plotted in Fig. 2.

[Fig. 1]

[Fig. 2]

It can be clearly seen that the Ce^{3+}-TiO_2 samples had a higher MBT adsorption capacity than TiO_2. While the saturated adsorption amount (Γ_{max}) of MBT onto the TiO_2 catalyst was 8.91×10^{-6} mol g^{-1}, the Γ_{max} of MBT onto the Ce^{3+}-TiO_2 catalysts increased with the increase of cerium ion content up to 19×10^{-6} mol g^{-1} about twice treatment of that adsorbed onto the TiO_2 catalyst. Of the Ce^{3+}-TiO_2 catalysts, 2.0% Ce^{3+}-TiO_2 achieved the highest Γ_{max} and K_a values. The factors leading to the enhanced adsorption ability should involve some changes of physical or chemical properties of the catalysts owing to the cerium ion doping. To further study the surface characteristics of the prepared catalysts, we carried out the BET analysis. The BET results showed that the specific surface areas of the catalysts increased from 43.29 m^2 g^{-1} for TiO_2 to 126.7 m^2 g^{-1} for 1.2% Ce^{3+}-TiO_2 significantly. The larger specific surface area of Ce^{3+}-TiO_2 catalysts would be beneficial to achieve better physical adsorption of MBT in aqueous suspension. Meanwhile, the cerium ion doping also changed the isoelectric point and the surface charge of catalysts. Lin et al.[29] reported the isoelectric point of ceria doped-TiO_2 was slightly lower than that of TiO_2. In this experimental condition of pH 6.25, MBT had a minor positive charge and Ce^{3+}-TiO_2 had a slightly negative charge. Thus the static adsorption between MBT and Ce^{3+}-TiO_2 could be favorable. In addition, the chemical adsorption between the Ce^{3+}-TiO_2 and MBT to form a complex of Ce^{3+}/Ce^{4+}-SH in the aqueous suspension

might play a more important role in this reaction. The complex of Ti^{4+}-SH could also be formed, but the equilibrium constant for the formation of Ti^{4+}-SH is much less than that of Ce^{3+}-SH [21].

3.2 Photocatalytic activity

To evaluate the effects of cerium ion dosage on the photocatalytic activity of Ce^{3+}-TiO_2, we carried out two sets of tests to degrade MBT in aqueous suspensions with an initial concentration of 0.28 mmol L^{-1} under UV illumination or 0.13 mmol L^{-1} under visible illumination by using different catalysts. The experimental results of MBT degradation with different catalysts are shown in Fig. 3A and B. The experiment demonstrated that all Ce^{3+}-TiO_2 catalysts achieved the higher rates of MBT degradation than did the TiO_2 catalyst. The enhancement of MBT degradation increased with the increase of Ce^{3+} content initially, but declined while the Ce^{3+} content reached a higher level. The results indicated that 1.2% Ce^{3+}-TiO_2 achieved the best performance under UV illumination and that 0.7% Ce^{3+}-TiO_2 performed best under visible light illumination. It can be seen that under visible light illumination, the MBT degradation in the TiO_2 suspension was insignificant, but MBT was successfully degraded in the Ce^{3+}-TiO_2 suspensions. The experimental results also indicated that the MBT degradation was considerably affected by the cerium ion content.

[Fig. 3]

To study the kinetics of MBT degradation in the aqueous suspension, we applied the Langmuir-Hinshelwood (L-H) model to describe the experimental data as follows:

$$-\frac{dC}{dt} = k_r \frac{K_a C}{1 + K_a C}$$

where $-\frac{dC}{dt}$ is the photodegradation rate of MBT, C is the MBT concentration in the solution, k_r is the reaction rate constant, K_a is the adsorption coefficient, and t is the reaction time.

Since we have obtained K_a values, both the apparent kinetic constant (K_{ap}) and photoreaction kinetic constant (k_r) of MBT degradation with different catalysts can be calculated by using the integral L-H model [30] of $Ln(C_0-C_t)+K_a(C_0-C_t)]$ vs t. The results are plotted vs. cerium ion dosage in Fig. 4A and B, respectively. Obviously, the dependence of K_r on cerium ion dosage was very similar to that of K_{ap}. The k_r value might be decisive to the overall photocatalytic rate.

[Fig. 4]

Compared to the photocatalytic activity under UV illumination, that of Ce^{3+}-TiO_2 catalysts under visible light illumination was significantly weaker. The lower efficiency of visible photo-degradation of MBT should be caused by lower optical absorbance in the range of 400-460 nm as shown in Fig. 8. It was noticeable that a stronger visual absorbance with a higher cerium ion dosage did not lead to a higher reaction rate, which might be limited by lower quantum efficiency. However, the specific value of quantum efficiency was not obtained in this study because of the limits of experimental conditions.

3.3 Crystal Structure

The XRD patterns of Ce^{3+}-TiO_2 samples as shown in Fig. 5 indicated that all samples had a similar pattern dominated by anatase. The relative intensity of the main anatase peak (101) decreased with the increase of Ce^{3+} content. This decrease might indicate that the cerium ion doping inhibited the TiO_2 phase transfer from amorphous structure to anatase, and that Ce^{3+}-TiO_2 had higher thermal stability than pure TiO_2. Additionally, no cerium oxides peaks were found in the XRD grams because of a low cerium dosage, although Reddy et al. [31] reported that CeO_2 was present in the 50% CeO_2-TiO_2 sintered at 773 K. In fact, the ionic radii of Ce^{3+} and Ce^{4+} are 1.03 and 1.02 Å, respectively, much bigger than that of Ti^{4+} (0.64 Å). Therefore, it is difficult for Ce^{3+}/Ce^{4+} to enter the lattice of TiO_2 structure although there was a very slight difference of the lattice parameter ‘c’ between the

TiO_2 and the Ce^{3+}-TiO_2 samples. Shah et al. [9] proposed that Nd^{3+} resides in the octahedral interstitial site of Nd^{3+}-TiO_2. In this study, the atomic ratio of Ce/Ti on the surface of the 0.7%, 1.2%, and 2.0% Ce^{3+}-TiO_2 samples was determined by the EDS analysis to be 1.16%, 1.59%, and 2.25%, respectively. These results showed that the amount of cerium ion on the surface of the Ce^{3+}-TiO_2 catalysts is higher that that in the bulk.

[Fig. 5]

[Table 1]

3.4 XPS Analyses

From the XPS analysis, the data of binding energy (BE), full width at a half of the maximum height of peaks (FWHM), and area percentage are listed in Table 2, while the Ti 2*p* XPS of 4 samples are shown in Fig. 6. It can be seen that the Ti 2*p* spectra of Ce^{3+}-TiO_2 showed a slight deformation in the lower side of binding energy, corresponding to the different oxidation states of Ti. In this investigation, the Ti $2p_{3/2}$ peak was well fitted into the two peaks of Ti^{4+} and Ti^{3+}. It was thought that reduction of Ti^{4+} to Ti^{3+} resulted from a charge imbalance caused by the cerium ion being localized in the octahedral interstitial site during heat treatment. From Fig. 6, it can be seen that the Ti $2p_{3/2}$ spectra of TiO_2 had an insignificant fitting peak at 457.04 eV representing Ti^{3+} and the Ti $2p_{3/2}$ spectra of Ce^{3+}-TiO_2 had more significant filling peaks between 457.58-457.86 eV representing Ti^{3+}. The fitting peaks at 458.70 eV represented Ti^{4+}. From Table 2, it can be clearly seen that the amount of Ti^{3+} on the surface of Ce^{3+}-TiO_2 catalysts increased considerably from 1.55% to 15.78% with the increase of cerium ion content from 0.7% to 2.0%, and the ratio of [O]/[Ti] decreased significantly with the increase of cerium ion content.

[Fig. 6]

[Table 2]

Recently a lot of efforts have been devoted to Ce 3*d* XPS interpretation by different researchers including Bensalem et al.[32], Larachi et al.[33], Reddy et al.[34-35], Park et al.[36], Rynkowski et al.[37], and Francisco et al.[38]. Two sets of spin-orbital multiplets corresponded to the $3d_{3/2}$ and $3d_{5/2}$ contributions. In this study, the Ce 3*d* XPS of 2.0% Ce^{3+}-TiO_2 catalyst are shown in Fig. 7. The peaks labeled "u" and "v" corresponded to Ce^{3+} and Ce^{4+} in ceria, respectively, in which the v_{01}, v_{11}, and v_{21} at 881.81, 886.82, and 896.45 eV represented Ce^{4+}, while the u_{01} and u_{11} at 885.72 and 880.81 eV represented Ce^{3+} in the Ce $3d_{5/2}$ spin-orbit split doublet. Correspondingly, the v_{02}, v_{12}, and v_{22} at 900.16, 904.77, and 913.49 eV represented Ce^{4+}, while the u_{02} and u_{12} at 902.16 and 897.95 eV represented Ce^{3+} in the Ce $3d_{3/2}$ spin-orbit split doublet, according to the results from Larachi et al. [33]. The structure of v_{01} and v_{11} was attributed to a mixture of $(5d\ 6s)^0\ 4f^2$ O $2p^4$ and $(5d\ 6s)^0\ 4f^1$ O $2p^5$ configurations between O 2*p* level and Ce 4*f* level, while v_{21} was a $(5d\ 6s)^0\ 4f^0$ O $2p^6$ final state. Similarly, the structure of u_{11} and u_{01} was attributed to a mixture of $(5d\ 6s)^0\ 4f^2$ O $2p^4$ and $(5d\ 6s)^0\ 4f^1$ O $2p^5$ configurations in Ce_2O_3.

[Fig. 7]

3.5 Photoresponse of TiO_2 and Ce^{3+}-TiO_2 under UV and visible light illumination

To investigate the optical absorption properties of catalysts, we examined the DRS of TiO_2 and Ce^{3+}-TiO_2 catalysts in the range of 220-850 nm and our results are shown in Fig. 8. The DRS results demonstrated that while TiO_2 had no absorption in the visible region (>400 nm), Ce^{3+}-TiO_2 had significant absorption between 400 and 500 nm, which increased with the increase of cerium ion content. In addition, it can be noted that the optical absorption in the UV region was also enhanced. In fact, the enhanced absorption in the visible region for the Ce^{3+}-doped Y_2O_3, Lu_2O_3, ZrO_2 or La_2O_3 had been reported and the onset of the predominant Ce^{3+} absorption was found at about 460 nm [24, 25]. CeO_2 is an n-type semiconductor with a band gap of about 3.2 eV [26, 39]. Therefore, the absorption at 400-500 nm by the Ce^{3+}-TiO_2 catalysts could not be attributed to CeO_2 but rather to Ce_2O_3. In contrast to the closed shell Ce^{4+} ion ($4f^0$), Ce^{3+} ion possesses a single optically-active

electron with the ground-state configuration in the $4f^1$ orbital. Within this configuration, there are only two electronic levels, an excited state of $^2F_{7/2}$ and a ground state of $^2F_{5/2}$. The 4*f*-4*f* transitions attributed to Ce^{3+} may only be observed in the infrared spectral region. However, Ce^{3+} has the first state configuration $5d^1$ that is rather close in energy. The electronic dipole transitions $4f^1 \leftrightarrow 5d^1$ may occur in either UV or visible region. Based on the valence band of Ce^{3+}-TiO_2 from XPS, it is proposed that electron-hole pairs could be generated in both types of catalysts: Ce^{3+}-TiO_2 and Ce_2O_3 in two approaches as shown in Fig. 9: (1) an electron can be excited from the valence band of Ce^{3+}-TiO_2 into Ce 4*f* level when the energy of photon is more than ($E_{ce4f} - E_v$), and (2) an electron can be excited from the ground state of Ce_2O_3 into Ce 4*f* level. Therefore, the red-shift of absorption edge for Ce^{3+}-TiO_2 was expressed in the following equations (1) and (2). The Ce 4*f* levels might play a crucial role in generating electron-hole pairs under visible light illumination.

$$Ce^{3+}\text{-}TiO_2 + h\nu \rightarrow e^- + h^+ \quad (1)$$

$$Ce_2O_3 + h\nu \rightarrow e^- + h^+ \quad (2)$$

[Fig. 8]

[Fig. 9]

3.5 Mechanism of Interfacial Charge Transfer

Wang and his co-workers had proven that the separation of electron-hole pairs is more efficient in the lanthanide ion-doped TiO_2 including La^{3+}, Nd^{3+}, Pr^{3+}, Sm^{3+}, and Eu^{3+} than that in pure TiO_2 [40, 41]. Interfacial charge transfer should be a determining-rate step for photocatalytic reaction [42]. In our investigation, the PL emission spectra of catalysts were studied to disclose the separation efficiency of charge carriers, because PL emission results from the recombination of free carrier. The PL emission spectra of all samples were examined in the range of 370-700 nm. The analytical results are shown in Fig. 10. It can be seen that the PL intensity of TiO_2 was significantly higher than that of

Ce^{3+}-TiO_2 samples. If we agree that the PL emission mainly results from the recombination of excited electron and holes, the lower PL intensity might indicate fewer recombinations between electron and holes. Of all catalysts, the PL intensity of 1.2% Ce^{3+}-TiO_2 was the lowest. That is the reason why the optimal dosage of ceria was 1.2% under UV light. In addition, the main PL peak of TiO_2 occurred at 524 nm, while those of Ce^{3+}-TiO_2 turned up at 538, 539, 541, and 551 nm, respectively. These results indicate that the position of PL peaks gradually shifted to the red direction with the increase of cerium ion content from 0.2 to 2.0%. This red shift of PL emission agreed with the red shift of UV-visible DRS.

[Fig. 10]

For Ce^{3+}-TiO_2, the Ce 4*f* level plays an important role in interfacial charge transfer and elimination of electron-hole recombination. Lanthanide ions could act as an effective electron scavenger to trap the CB electrons of TiO_2. Lanthanide ions, acting as a Lewis acid, apparently were superior to the oxygen molecule (O_2) in the capability of trapping CB electrons [27, 43]. The electrons trapped in Ce^{4+}/Ce^{3+} site was subsequently transferred to the surrounding adsorbed O_2. The presence of Ce^{4+} on TiO_2 surface may promote the following processes expressed by Equations 3 and 4. The formation of •OH might be proposed as Equation 5 and then a photogenerated electron was transferred efficiently. For Ce^{3+}-TiO_2, the formation of labile oxygen vacancies and particularly the relatively high mobility of bulk oxygen species have been reported [31], so ceria had a high oxygen transport and storage capacity [43]. Hence, the excited electrons might be more easily transferred to O_2 on the surface of Ce^{3+}-TiO_2 catalysts.

$$Ce^{4+} + TiO_2\,(e^-) \rightarrow Ce^{3+} + TiO_2 \quad (3)$$

$$Ce^{3+} + O_2 \rightarrow O_2^- + Ce^{4+} \quad (4)$$

$$O_2^{\bullet-} + 2H^+ \rightarrow 2\bullet OH \quad (5)$$

On the other hand, Ti^{3+} can also form a defect level and act as the hole-traps to promote the charge transfer. These defects on the TiO_2 surface or in its bulk can suppress the recombination of electron-hole pairs and hence extend their lifetime. The mechanism of interfacial charge transfer can be expressed in Equations 6 and 7 [45, 46].

$$Ti^{4+}\text{-O-H} + e^- \rightarrow Ti^{3+}\text{-O-H}^- \quad (6)$$

$$Ti^{3+}\text{-O-H}^- + h^+ \rightarrow Ti^{4+}\text{-}^{\bullet}\text{O-H} \quad (7)$$

However, to certain degree, the higher content of Ti^{3+} on the Ln^{3+}-TiO_2 surface compared to that of TiO_2 would accelerate the interfacial charge transfer and enhance the photocatalytic activity. But the content of Ti^{3+} should have an optimal range. In the present study, it was found that the Ti^{3+} content increased with the increase of Ce^{3+} dosage. However, the defect level would become the recombination center of electron-hole pairs and lead to the decrease of photocatalytic activity, when Ti^{3+} content exceeded its optimal value. The optimal dosage of cerium ion under visible light illumination was found to be 0.7%, while that under UV illumination was 1.2%. Ikeda and his co-workers [20] proposed that the rate of electron-hole escaping from their recombination should be proportional to the light flux of excitation and to the probability of light absorption to produce an electron-hole (Φ). This means the optimal dosage might be dependent on reaction conditions. The value of Φ under visible light illumination is much lower than that under UV illumination in this study. The lower Φ value might lead to the lower Ti^{3+} content. Therefore, the optimal dosage of ceria under visible light illumination was less than that UV illumination in this experimental condition.

4. Conclusions

The overall photocatalytic activity for MBT degradation under UV or visible light irradiation was signficiantly enhanced by doping with the cerium ions with a special 4*f* electron configuration because the higher adsorption equilibrium constant and the higher separation efficiency of electron-hole pairs were obtained simultaneously for Ce^{3+}-TiO_2 catalysts. The introduction of Ce 4*f* level led to the optical absorption band between 400-500 nm. The formation of two sub-energy levels (defect

level and Ce 4*f* level) in Ce^{3+}-TiO_2 might be a critical reason to eliminate the recombination of electron-hole pairs and to enhance the photocatalytic activity under UV or visible light illumination.

Acknowledgement

The authors wish to thank the Hong Kong Polytechnic University for some financial support of this work under a Postdoctoral Fellowship Grant (Project No.: G-YW69/02) and China National Natural Science Foundation Project No. 20203007. The authors would also like to extend their thanks to Dr. Liu H. and Prof. Yu J. G. for their revision suggestions.

References

〔1〕 A. Fujishima, T. N. Rao, D. A. Tryk, J. Photochem. Photobiol. C: Photochem. Rev. 1 (2000) 1.

〔2〕 P. V. Kamat, Chem. Rev. 1993, 93, 267.

〔3〕 M. R. Hoffmann, S. T. Martin, W. Choi, D. W. Bahnemann, Chem. Rev. 95 (1995) 69.

〔4〕 X. Z. Li, F. B. Li, Environ. Sci. Technol. 35 (2001) 2381.

〔5〕 J. G. Yu, J. C. Yu, M. K. P. Leung, W. K. Ho, B. Cheng, X. J. Zhao, J. C. Zhao, J. Catal. 217 (2003) 69.

〔6〕 J. G. Yu, H. G. Yu, B. Cheng, X. J. Zhao, J. C. Yu, W. K. Ho, J. Phys. Chem. B 107 (2003) 13871.

〔7〕 A. D. Paola, G. Marci, L. Palmisano, M. Schiavello, K. Uosaki, S. Ikeda, B. Ohtani, J. Phys. Chem. B 106 (2002) 637.

〔8〕 J. G. Yu, J. C. Yu, B. Cheng, X. J. Zhao, J. Sol-Gel Sci. Technol. 24 (2002) 39.

〔9〕 S. I. Shah, W. Li, C.-P. Huang, O. Jung, C. Ni, PNAS. 99 (2002) 6482.

〔10〕J.A. Wang, R. Limas-Ballesteros, T. Lopez, A. Moreno, R. Gomez, O. Novaro, X. Bokhimi, J. Phys. Chem. B 105 (2001) 9692.

〔11〕U. Diebold, H.-S. Tao, N. D. Shinn, T.E. Madey, Phys. Rev. B 50 (1994) 14474.

〔12〕P. V. Kamat, J. Phys. Chem. B 106 (2002) 7729.

〔13〕M. Jakob, H. Levanon, P. V. Kamat, Nano Lett. 3 (2003) 353.

〔14〕F.B. Li, X. Z. Li, Appl Catal A: Gen. 228 (2002) 15.

〔15〕E. Bae, W. Choi, Environ. Sci. Technol. 37 (2003) 147.

〔16〕M. Miyauchi, A. Nakajima, T. Watanabe, K. Hashimoto, Chem. Mater. 14 (2002) 4714.

〔17〕X. Z. Li, F. B. Li, C. L. Yang, W. K. Ge, J. Photochem. Photobiol. A: Chem. 141 (2001) 209.

〔18〕B. M. Reddy, P. M. Sreekanth, E. P. Reddy, Y. Yamada, Q. Xu, H. Sakurai, T. Kobayashi, J. Phys. Chem. B 106 (2002) 5695.

〔19〕A. Furube, T. Asahi, H. Masuhara, H. Yamashita, M. Anpo, J. Phys. Chem. B 103 (1999) 3120.

〔20〕S. Ikeda, N. Sugiyama, B. Pal, G. Marcí, L. Palmisano, H. Noguchi, K. Uosaki, B. Ohtani, Phys. Chem. Chem. Phys. 3 (2001) 267.

〔21〕K. T. Ranjit, I. Willner, S. H. Bossmann, A. M. Braun, J. Catal. 204 (2001) 305.

〔22〕K. T. Ranjit, I. Willner, S. H. Bossmann, A. M. Braun, Environ. Sci. Technol. 35 (2001) 1544.

〔23〕Y. B. Xie, C. W. Yuan, Appl. Surf. Sci. 221 (2004) 17.

〔24〕V. M. Orera, R. I. Merino, F. Pena, Solid State Ionics 72 (1994) 224.

〔25〕W. M. Yen, M. Raukas, S. A. Basun, W. V. Schaik, U. Happek, Journal of Luminescence 69 (1996) 287.

〔26〕B. Elidrissi, M. Addou, M. Regragui, C. Monty, A. Bougrine, A. Kachouane, Thin Solid Films 379 (2000) 23.

〔27〕J. M. Coronado, A. J. Maria, A. Martínez-Arias, J. C. Conesa, J. Soria, J. Photochem. Photobiol. A: Chem. 150 (2002) 213.

〔28〕I. Langmuir, J. Am. Chem. Soc. 40 (1918) 1361.

〔29〕J. Lin, J. C. Yu, J. Photochem. Photobiol. A: Chem. 116 (1998) 63.

〔30〕F. B. Li, X. Z. Li, K. H. Ng, Appl. Catal. B: Environ. (Under Review).

〔31〕B. M. Reddy, A. Khan, Y. Yamada, T. Kobayashi, S. Lordant, J.-C. Volta, J. Phys. Chem. B 107 (2003) 5162.

〔32〕A. Bensalem, F. Bozon-Verduraz, M. Delamar, G. Bugli, Appl. Catal. A: Gen. 121 (1995) 81.

〔33〕F. Larachi, J. Pierre, A. Adnot, A. Bernis, Appl. Surf. Sci. 195 (2002) 236.

〔34〕B. M. Reddy, A. Khan, Y. Yamada, T. Kobayashi, S. Lordant, J.-C. Volta, J. Phys. Chem. B 106 (2002) 10964.

〔35〕B. M. Reddy, A. Khan, Y. Yamada, T. Kobayashi, S. Lordant, J.-C. Volta, Langmuir 19 (2003) 3025.

〔36〕P. W. Park, J. S. Ledford, Langmuir 12 (1996) 1794.

〔37〕J. Rynkowski, J. Farbotko, R. Touroude, L. Hilaire, Appl. Catal. A: Gen. 203 (2000) 335.

〔38〕M. S. P. Francisco, V. R. Mastelaro, J. Phys. Chem. B 105 (2001) 10515.

〔39〕S. Y. Zheng, A. M. Andersson-Faldt, C. G. Granqvist, Appl. Opt. 32 (1993) 6303.

〔40〕Y. Q. Wang, H. M. Cheng, Y. Z. Hao, J. M. Ma, W. H. Li, S. M. Cai, Thin Solid Films 349 (1999) 120.

〔41〕Y. Q. Wang, H. M. Cheng, Y. Z. Hao, J. M. Ma, W. H. Li, S. M. Cai, Mater. Sci. Lett. 18 (1999) 127.

〔42〕H. Liu, X. Z. Li, Y. J. Leng, W. Z. Li, J. Phys. Chem. B 107 (2003) 8988.

〔43〕Y. B. Xie, C. W. Yuan, Appl. Catal. B: Environ. 46 (2003) 251.

〔44〕Y. Namai, K-i. Fukui, Y. Iwasawa, J. Phys. Chem. B 107 (2003) 11666.

〔45〕S. H. Szczepankiewicz, J. A. Moss, M. R. Hoffmann, J. Phys. Chem. B. 106 (2002) 2922.

〔46〕S. H. Szczepankiewicz, J. A. Moss, M. R. Hoffmann, J. Phys. Chem. B. 106 (2002) 7654.

Table 1. Crystal parameters of Ce^{3+}-TiO_2 catalysts

Ce content (10^{-2} mol/mol)	0	0.2	0.7	1.2	2.0
Crystal pattern	Anatase	Anatase	Anatase	Anatase	Anatase
Crystal size (nm)	32.90	20.15	10.07	9.16	10.07
Crystal lattice "a" (Å)	3.780	3.778	3.774	3.780	3.784
Crystal lattice "c" (Å)	9.502	9.456	9.480	9.480	9.480
Crystal volume ($Å^3$)	135.77	134.97	135.02	135.45	135.74

Table 2: XPS fitting data for TiO_2 and Ce^{3+}-TiO_2 catalysts

Catalysts	O/Ti	Ti 2p 3/2					
		Ti^{3+}			Ti^{4+}		
		BE (eV)	FWHM (eV)	Area (%)	BE (eV)	FWHM (eV)	Area (%)
TiO_2	2.11	457.04	1.13	0.16	458.70	1.08	99.86
0.7% Ce^{3+}-TiO_2	1.82	457.05	1.01	1.55	458.70	1.08	98.45
1.2% Ce^{3+}-TiO_2	1.73	457.43	1.03	5.64	458.70	1.08	94.36
2.0% Ce^{3+}-TiO_2	1.49	457.63	1.02	15.78	458.70	1.10	84.22

FWHM: Full width at a half of the maximum height of peaks; BE: Binding energy

List of figure captions

Fig. 1: The MBT adsorption isotherms on the different catalysts obtained by plotting the equilibrium concentration (C_e) versus the adsorbed amounts of MBT (Γ).

Fig. 2: The adsorption equilibrium constant, K_{ap} and the saturated adsorption amount, Γ_{max} vs. cerium ion dosage.

Fig. 3: The photocatalytic degrdation of MBT with an initial concentration of 0.28 mmol L^{-1} using different catalysts under UV irradiation (A) and with an initial concentration of 0.13 mmol L^{-1} under visible light irradiation (B).

Fig. 4: The apparent kinetic constant, k_{ap} (A) and the photoreaction kinetic constant, k_r (B) vs. cerium ion dosage.

Fig. 5: The XRD photograph of TiO_2 and Ce^{3+}-TiO_2 catalysts.

Fig. 6: The Ti 2p XPS spectra of TiO_2 and Ce^{3+}-TiO_2 catalysts, A: TiO_2; B: 0.7% Ce^{3+}-TiO_2; C: 1.2% Ce^{3+}-TiO_2; D: 2.0% Ce^{3+}-TiO_2.

Fig. 7: The Ce 3d XPS spectroscopy of 2.0% Ce^{3+}-TiO_2 catalyst.

Fig. 8: The UV-visible diffuse reflectance spectra of TiO_2 and Ce^{3+}-TiO_2 catalysts.

Fig. 9: The photoluminescence emission spectra of TiO_2 and Ce^{3+}-TiO_2 catalysts at 77 K.

Fig. 10: The proposed valence band structure of Ce^{3+}-TiO_2 and the mechanisms of photoresponse under visible light and photogenerated electron transfer.

Fig. 1

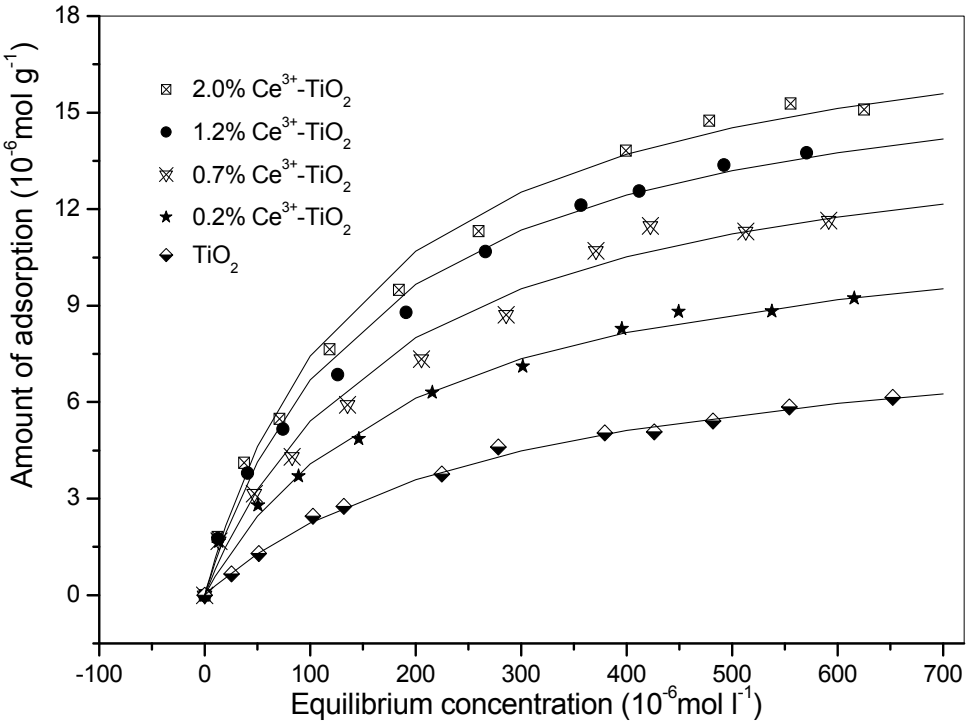
2.0% Ce3+-TiO2
1.2% Ce3+-TiO2
0.7% Ce3+-TiO2
0.2% Ce3+-TiO2
TiO2
Amount of adsorption (10-6mol g-1)
Equilibrium concentration (10-6mol l-1)
18
15
12
9
6
3
0
-100
0
100
200
300
400
500
600
700

Fig. 2

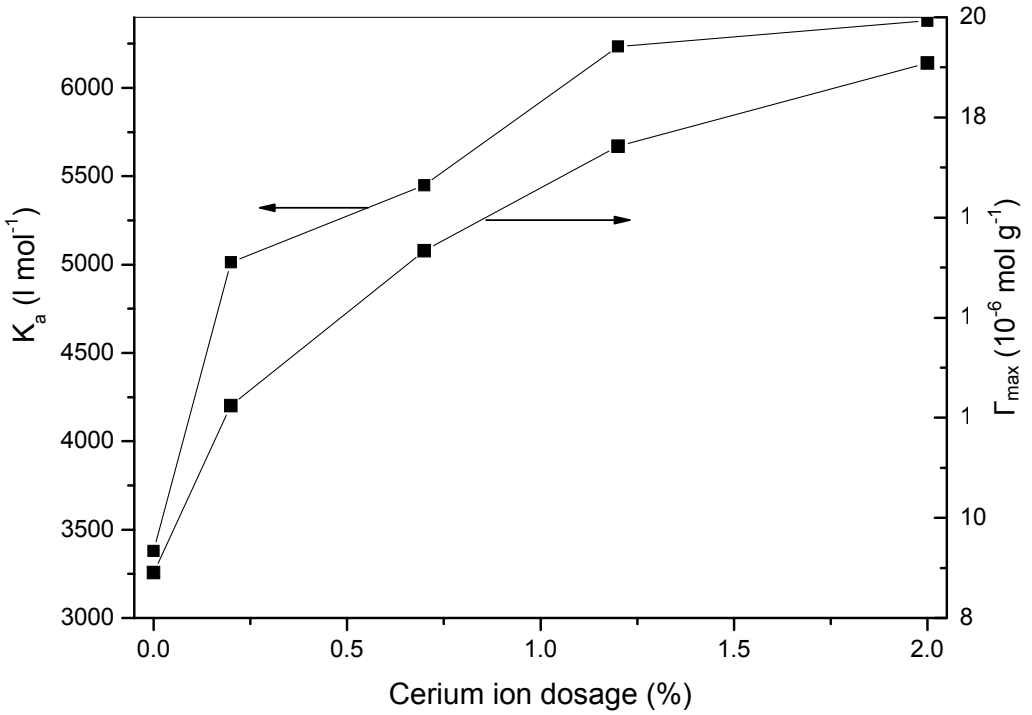
6000
5500
5000
4500
4000
3500
3000
K_a (l mol^{-1})
20
18
1
1
1
10
8
Γ_{max} (10^{-6} mol g^{-1})
0.0
0.5
1.0
1.5
2.0
Cerium ion dosage (%)

Fig. 3

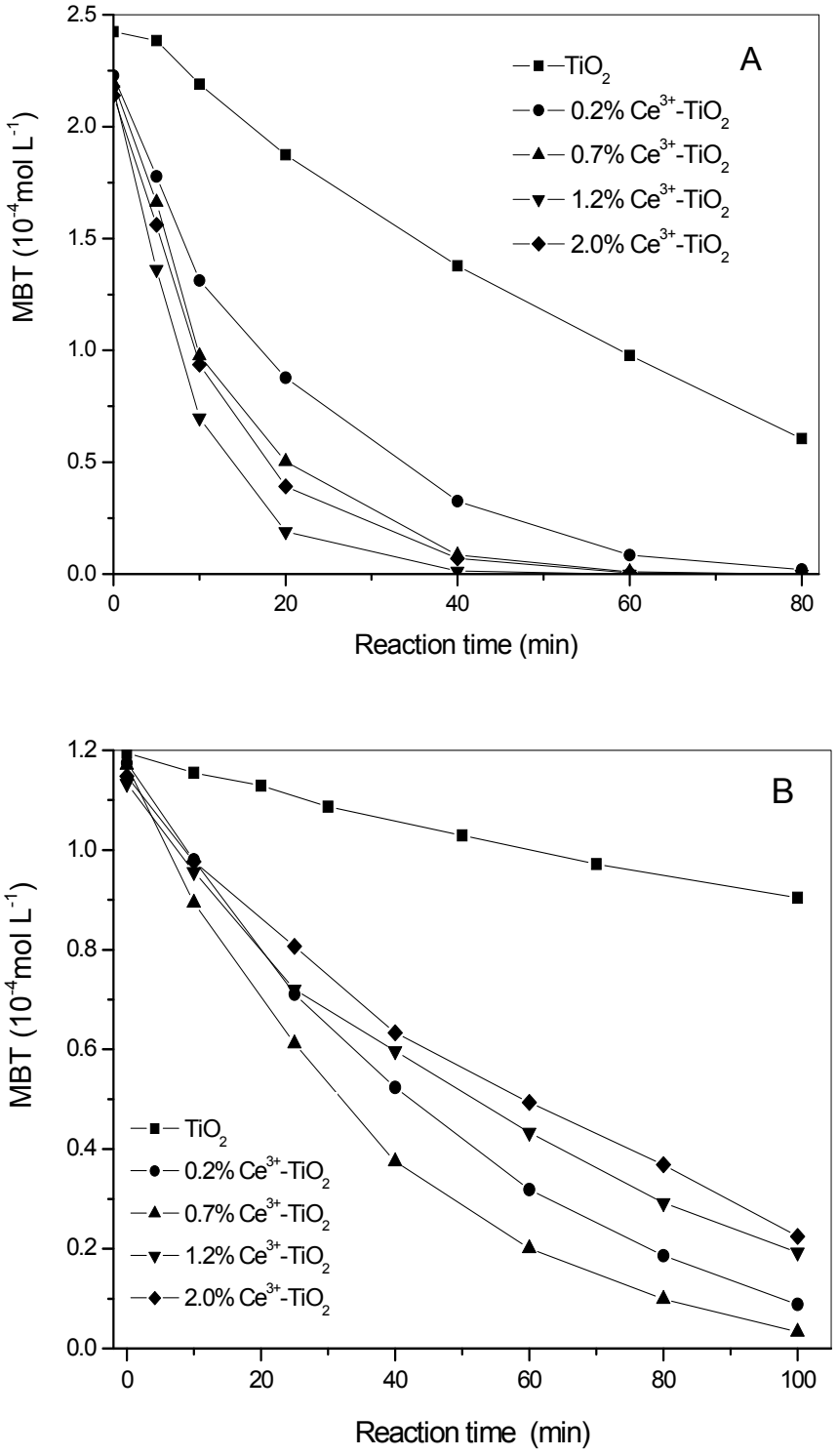
A
TiO2
0.2% Ce3+-TiO2
0.7% Ce3+-TiO2
1.2% Ce3+-TiO2
2.0% Ce3+-TiO2
MBT (10-4mol L-1)
Reaction time (min)
B
TiO2
0.2% Ce3+-TiO2
0.7% Ce3+-TiO2
1.2% Ce3+-TiO2
2.0% Ce3+-TiO2
MBT (10-4mol L-1)
Reaction time (min)

Fig. 4

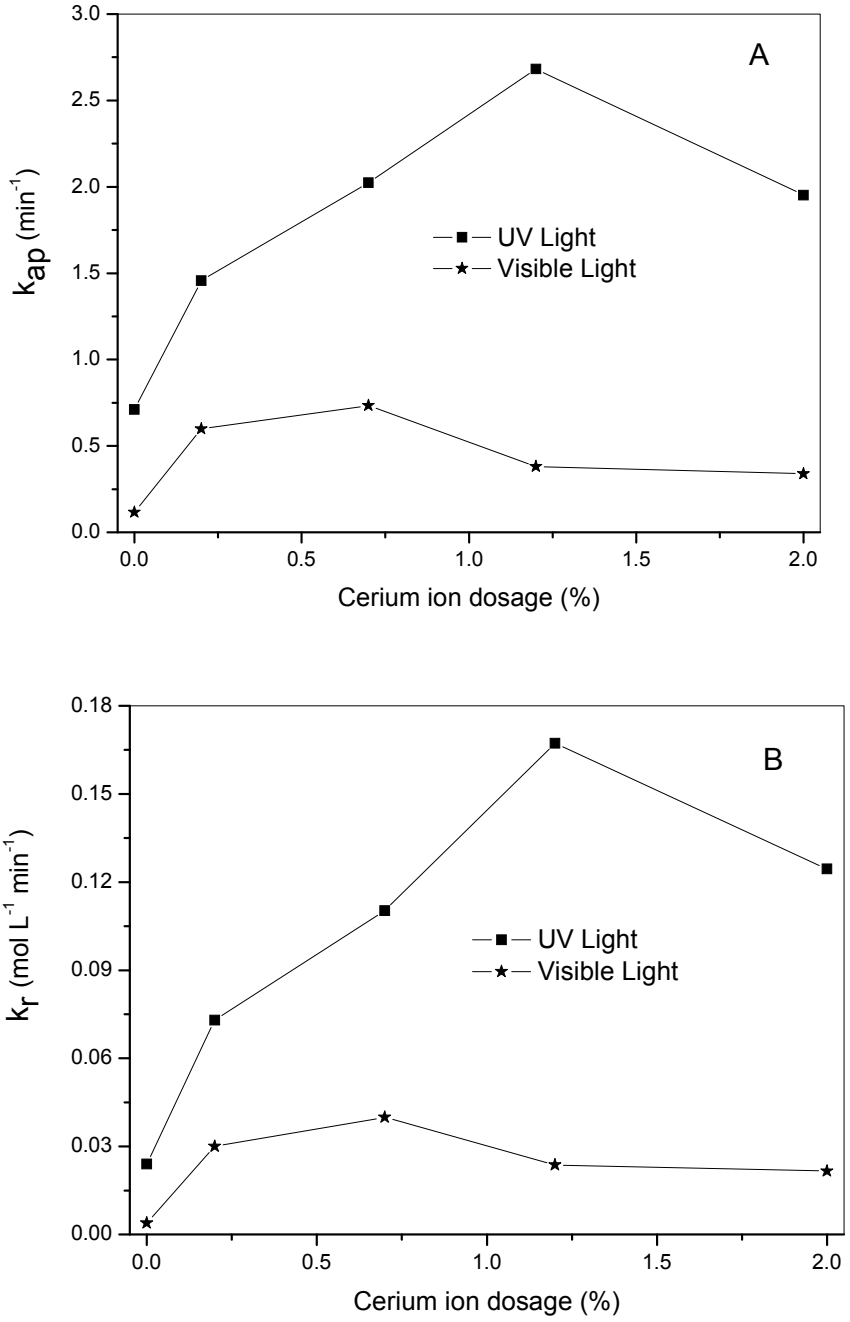
A
B
UV Light
Visible Light
k_{ap} (min^{-1})
k_r (mol L^{-1} min^{-1})
Cerium ion dosage (%)
Cerium ion dosage (%)

Fig. 5

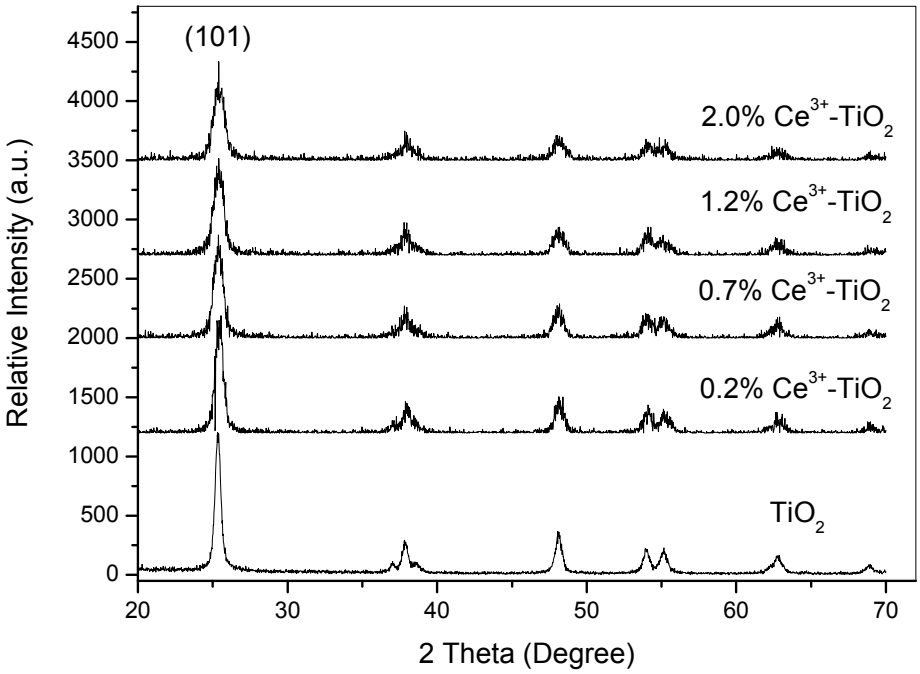
(101)
2.0% Ce3+-TiO2
1.2% Ce3+-TiO2
0.7% Ce3+-TiO2
0.2% Ce3+-TiO2
TiO2
Relative Intensity (a.u.)
2 Theta (Degree)
0
500
1000
1500
2000
2500
3000
3500
4000
4500
20
30
40
50
60
70

Fig.6

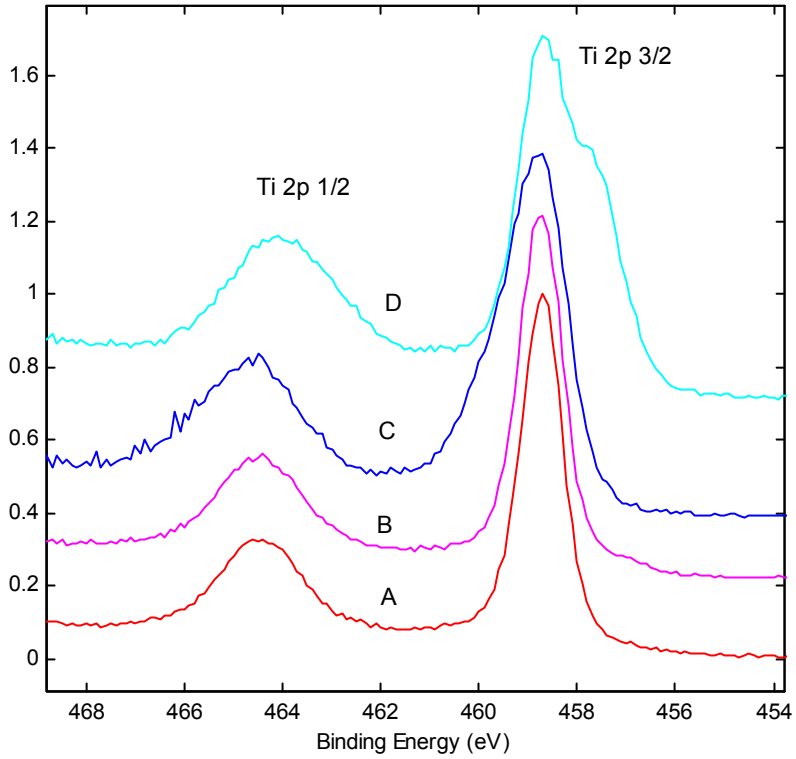
Ti 2p 3/2
Ti 2p 1/2
D
C
B
A
1.6
1.4
1.2
1
0.8
0.6
0.4
0.2
0
468
466
464
462
460
458
456
454
Binding Energy (eV)

Fig. 7

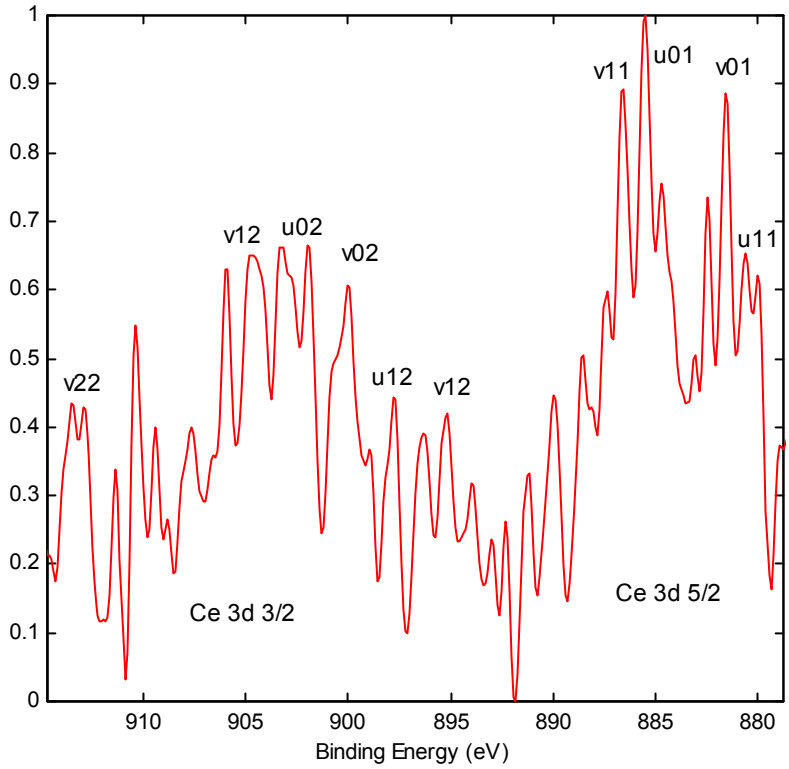
1
0.9
0.8
0.7
0.6
0.5
0.4
0.3
0.2
0.1
0
910
905
900
895
890
885
880
Binding Energy (eV)
v22
v12
u02
v02
u12
v12
v11
u01
v01
u11
Ce 3d 3/2
Ce 3d 5/2

Fig. 8

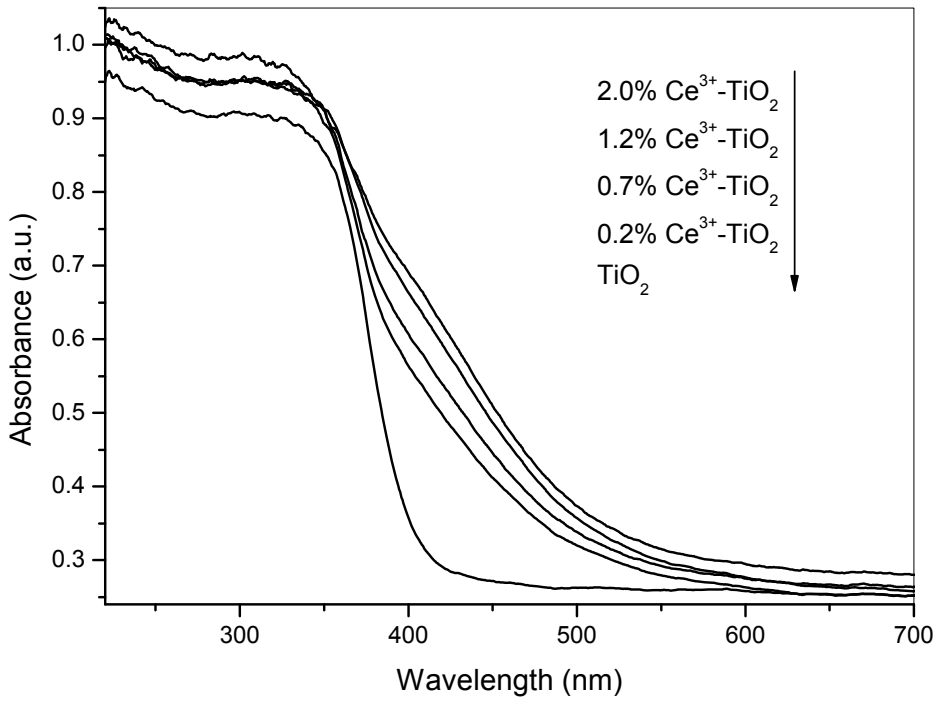
Absorbance (a.u.)
Wavelength (nm)
2.0% Ce3+-TiO2
1.2% Ce3+-TiO2
0.7% Ce3+-TiO2
0.2% Ce3+-TiO2
TiO2

Fig. 9

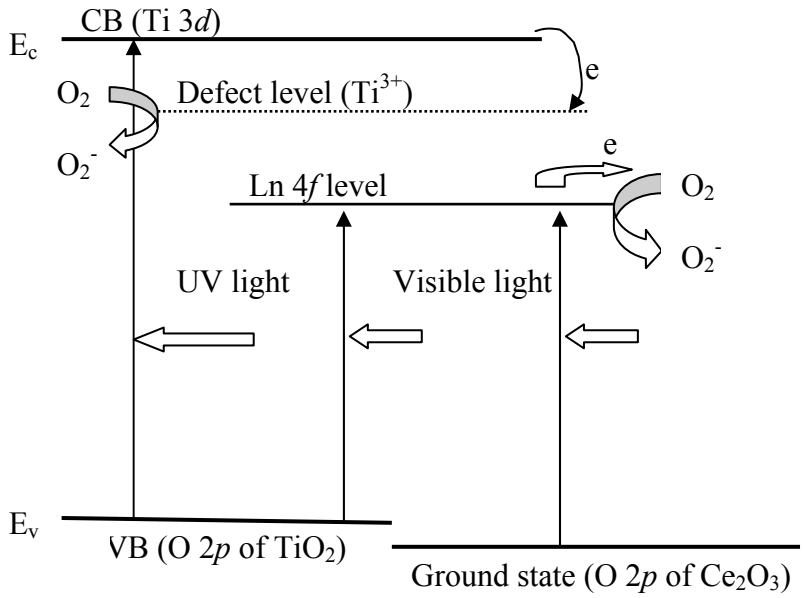
CB (Ti 3d)
E_c
e
O_2
Defect level (Ti^{3+})
O_2^-
e
Ln 4f level
O_2
O_2^-
UV light
Visible light
E_v
VB (O 2p of TiO_2)
Ground state (O 2p of Ce_2O_3)

Fig. 10

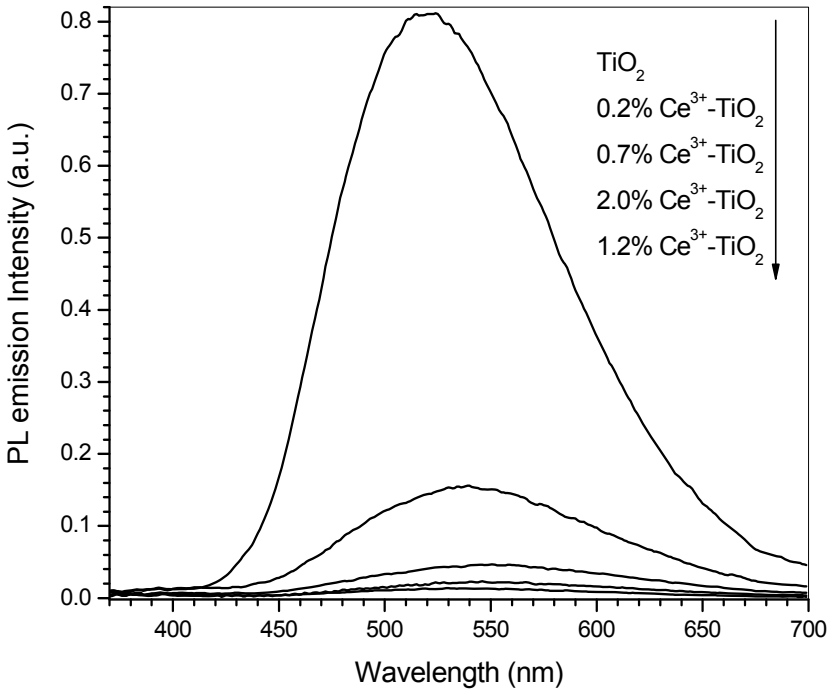
PL emission Intensity (a.u.)
Wavelength (nm)
0.0
0.1
0.2
0.3
0.4
0.5
0.6
0.7
0.8
400
450
500
550
600
650
700
TiO2
0.2% Ce3+-TiO2
0.7% Ce3+-TiO2
2.0% Ce3+-TiO2
1.2% Ce3+-TiO2